Calibration and optimization of computer-controlled optical surfacing for large optics

Dae Wook Kim*[a], Hubert M. Martin[b], James H. Burge[a, b]
[a]College of Optical Sciences, Univ. of Arizona, Tucson, AZ 85721, USA;
[b]Steward Observatory, University of Arizona, Tucson, AZ 85721, USA

ABSTRACT

Precision optical surfaces can be efficiently manufactured using a computer-controlled optical surfacing (CCOS) process. Most CCOS processes are based on control of the dwell time of a tool on the workpiece, according to the desired removal and the tool influence function (TIF), which is the material wear function of the tool. Several major topics were investigated to improve current CCOS processes and provide new solutions for the next generation of CCOS processes. A rigid conformal (RC) lap using a visco-elastic non-Newtonian medium was invented. It conforms to the aspheric surface shape, yet maintains stiffness on short time scales to provide natural smoothing. The smoothing removes mid- to high-frequency errors while controlled dwell time removes low-frequency errors. A parametric smoothing model was also introduced to predict the smoothing effects. A parametric edge TIF model to represent measured edge TIFs was developed and demonstrated. This model covers the removal behavior as the tool overhangs the edge of the workpiece. These new tools and models were applied in a new process optimization technique called non-sequential optimization. The non-sequential approach performs a comprehensive optimization of dwell time using multiple TIFs (multiple tools) simultaneously. An overview of these newly implemented CCOS features** is presented along with some actual CCOS results.

Keywords: Computer-controlled optical surfacing, rigid conformal lap, smoothing model, edge TIF, non-sequential optimization

1. INTRODUCTION

Various computer-controlled optical surfacing (CCOS) processes have been developed since the 1960s [1-9]. These CCOS processes can provide good solutions for fabrication of precision optics because of their high convergence rates based on deterministic removal processes. Many large aspheric optical surfaces and off-axis segments have been successfully fabricated using these CCOS techniques [4-9]. Nevertheless, further development in the efficiency and performance of the current CCOS techniques is desired to meet the demanding target specifications of many next-generation optical systems, which usually have hundreds of aspheric mirrors (e.g. Thirty Meter Telescope (TMT) [10], European Extremely Large Telescope (EELT) [11] and Laser Inertial Fusion Engine (LIFE) [12]) or large off-axis mirrors (e.g. Giant Magellan Telescope (GMT) [13]).

Telescopes such as TMT and EELT use giant segmented primary mirrors with hundreds of square meters of collecting area, and may have hundreds of segments. Each meter-class segment assembly is to have the maximum overall wavefront RMS (root-mean-square) amplitude of <100nm [14]. The next-generation CCOS process needs to fabricate such precision optical surfaces in a highly efficient manner. In addition to the superb figuring ability, suppression of mid-spatial-frequency error on these precision optical surfaces is important for maximum performance of the optical systems (i.e. less scattering and well defined point spread function) [15]. Most of the recent large optical surfaces have been polished until the surface errors satisfied a target structure function or power spectral density specification to quantify the form accuracy as a function of spatial frequency [15-16].

*letter2dwk@hotmail.com

** We have reported these new CCOS technologies in various papers separately. The purpose of this paper is to summarize the technologies in one piece, and provide some measured results. Sections 1 and 2 are mainly from the previous publications without major changes [18, 21-25].

Optical Manufacturing and Testing IX, edited by James H. Burge, Oliver W. Fähnle, Ray Williamson,
Proc. of SPIE Vol. 8126, 812615 · © 2011 SPIE · CCC code: 0277-786X/11/$18 · doi: 10.1117/12.893878

The popularity of segmented optics has also increased the demand for an efficient edge figuring process. Those next-generation systems have multiple mirror segments as their primary or secondary mirrors, the total length of edges is much larger than in the conventional system with one mirror, and the edges are distributed across the whole pupil. Thus a precise and efficient edge fabrication method is important to ensure the final performance of the optical system and reasonable delivery time. Therefore, the improved next-generation CCOS technique must provide an efficient fabrication process for mass-fabrication of precision aspheric optical surfaces.

Most CCOS processes are based on three main components: i) a numerically controlled (NC) polishing machine, ii) a polishing tool, and iii) an embedded process control intelligence. The NC polishing machine provides a stable and repeatable control environment to move the polishing tool on a workpiece. The polishing tool needs to provide a deterministic tool influence function (TIF), which is the shape of the wear function created by the polishing tool motion and workpiece motion. This well characterized TIF is usually mathematically modeled and used as a building block in the process control intelligence. The embedded process control intelligence designs and optimizes polishing run parameters, such as tool speed, tool pressure, and dwell time map (i.e. tool ablation time as a function of tool position on a workpiece), to achieve a target removal map. This paper summarizes some newly developed CCOS technologies at the University of Arizona, and provides actual polishing results using the advanced CCOS processes.

2. ADVANCED CCOS TECHNOLOGY

2.1 Rigid Conformal Lap

The TIF, which is the building block for a CCOS process, is a direct function of tool properties, such as pressure distribution under the tool, tool contact area shape, tool motion, and so forth. Thus, developing a well-behaved tool is an essential component to achieve a deterministic TIF. Tool development for highly aspheric optics production is an especially complex problem. Because local curvatures of an aspheric surface vary as a function of position on a workpiece, a tool with a rigid surface shape cannot be used. Instead, flexibility is required to maintain intimate contact with the workpiece surface, and not to leave zones in the workpiece surface figure due to the tool-workpiece misfit. However, the smoothing effect that naturally removes mid- to high-spatial-frequency errors by a rigid tool rubbing high portions on a rough surface disappears as the tool becomes too compliant [17].

The rigid conformal (RC) lap, which uses a visco-elastic non-Newtonian fluid (a.k.a. solid-liquid) that has both flexibility and rigidity, was developed and introduced in 2010 [18]. A schematic RC lap structure is shown in Fig. 1.

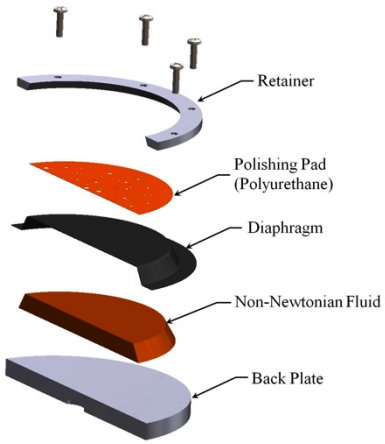

Fig. 1. 3D schematic Rigid Conformal lap structure (exploded and cut in half) [18]. Note: A US provisional patent was filed for the RC lap.

The RC lap has the advantages of both rigid and compliant tools for different time scales. It can be used just like a rigid tool, which has natural smoothing effects, for relatively fast tool motion (e.g. orbital motion). As it moves along the tool path on a workpiece, the non-Newtonian fluid flows to fit the slowly varying local curvatures under the tool. Highly deterministic TIFs and removal rate were experimentally demonstrated. The measured data showed TIF stability of <10% and superb surface finish with <10Å roughness on a ULE substrate [18]. In addition to its good performance, the

ease with which a large tool can be made in a cost-effective manner makes the RC lap an attractive solution for large aspheric precision optics manufacturing.

The RC lap has been successfully used in many CCOS projects at the Optical Engineering and Fabrication Facility (OEFF) and Steward Observatory Mirror Lab (SOML) at the University of Arizona since 2010 [19-20].

2.2 Parametric Smoothing Model

The smoothing effect becomes more important for large workpiece fabrication, because it is almost the only way to correct high-spatial-frequency errors smaller than the tool size. Based on the deterministic TIFs of CCOS processes, errors on scales larger than the tool size can be corrected by increasing the dwell time on the high areas. However, this method cannot be used for small-scale and mid-scale errors unless smaller and smaller tools are used. Smaller tools require much higher tool positioning accuracy to avoid residual tool marks, which is another source of mid-spatial-frequency errors. Also, the use of small tools increases the overall fabrication time.

Correcting these mid- to high-spatial-frequency errors on the optical surfaces is very important for next-generation extremely large telescopes [10-11, 13] and nuclear fusion energy plants using high-power lasers (e.g. LIFE [12]). Because the mid- to high-spatial-frequency errors affect the sharpness of the point spread function or the scattering characteristic of high-power laser application optics, the overall performance of those systems may be degraded due to these errors.

A parametric smoothing model to quantitatively describe the smoothing effects was developed and reported in 2010 [21]. This model uses a parametric approach to include other effects such as fluid dynamics of the polishing compound and total effective stiffness of the whole tool structure. Two experimental smoothing results by a conventional pitch tool and the RC lap are clearly demonstrated in Fig. 2 [21].

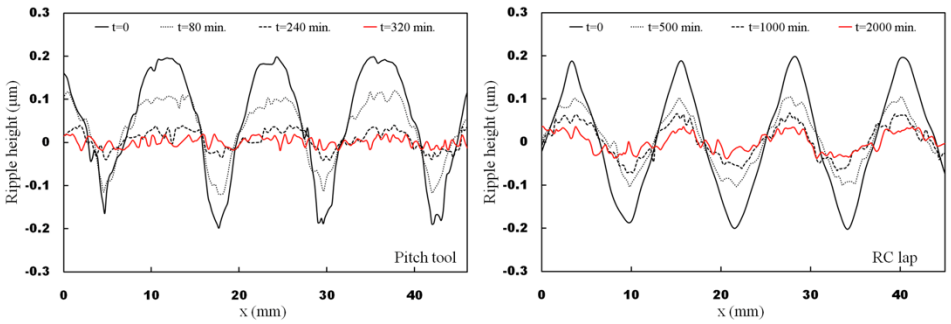

Fig. 2. Measured ripple profiles (t = accumulated smoothing run time) as tool smoothes out the ripples on glass substrates: pitch tool (left) and RC lap (right) [21] (Note: The tool diameter (100mm) was much larger than the period of the ripple.)

This smoothing model can be used to enhance the CCOS convergence rate by predicting the smoothing effects in a CCOS simulation.

2.3 Edge Tool Influence Function Model

In order to develop a CCOS process for edge figuring, accurate edge TIF models to represent the measured edge TIFs are required. A theoretical TIF can be calculated based on the equation of material removal, Δz, which is known as Preston's equation,

$$\Delta z(x,y) = \kappa \cdot P(x,y) \cdot V_T(x,y) \cdot \Delta t(x,y) \tag{1}$$

where Δz is the integrated material removal from the workpiece surface, κ the Preston coefficient (i.e. removal rate), P pressure on the tool-workpiece contact position, V_T magnitude of relative speed between the tool and workpiece surface and Δt dwell time. It assumes that the integrated material removal, Δz, depends on P, V_T and Δt linearly.

A nominal TIF calculated by integrating Eq. (1) under a moving tool fits well to an experimental (i.e. measured) TIF as long as the tool stays inside the workpiece. However, once the tool overhangs the edge of workpiece, Eq. (1) cannot be used because P varies strongly over the contact area in a complex way, the assumptions of linearity may not be valid,

and the shape of the tool surface may vary due to bending, compression and flow. An empirically determined TIF is needed.

A parametric edge TIF model using two correction terms was introduced to model the edge TIFs in 2009 [22-23]. Rather than assigning the edge effects to a certain type of analytical pressure distribution model, we define a parametric model based on measured data that allows us to create an accurate TIF without the need of identifying the actual cause of the abnormal behavior in edge removal. The performance evaluation for the parametric edge TIF model was conducted by comparing the model and measured edge TIFs as shown in Fig.3 [22].

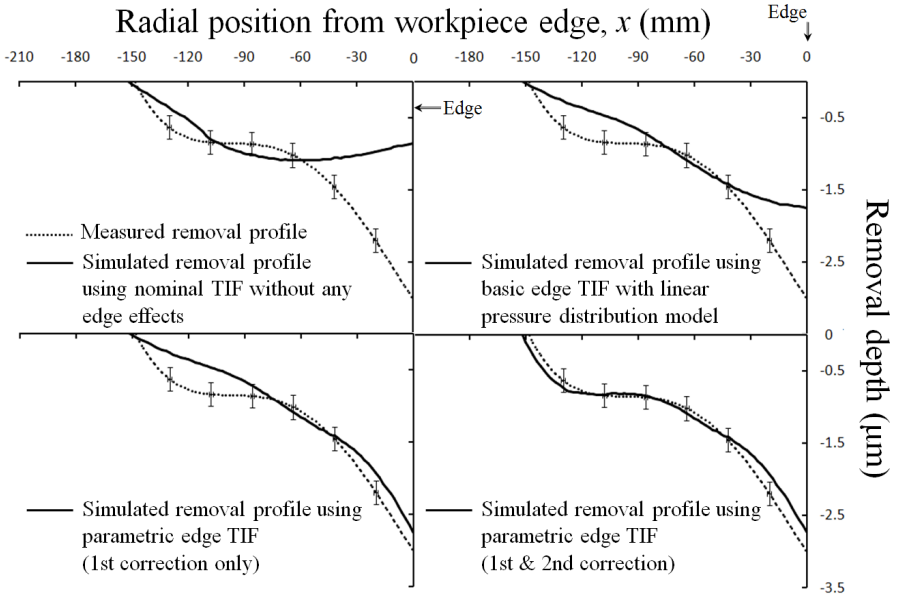

Fig. 3. Measured (with RMS error bars) vs. simulated (using different edge TIF models) edge removal profiles for the orbital tool motion case [22].

As shown in Fig. 3, the simulated removal profile based on the nominal TIF (edge effects ignored, top left) does not follow the overall slope of the measured removal profile. Especially, it shows a large difference in the edge-side removal starting about 50mm from the edge. The basic edge TIF (top right) assumes a linear pressure distribution that balances net force and moment. It comes closer to matching the slope of the measured removal. However, two mismatches between the measured and simulated removal are clearly observed in the edge-side and workpiece-center-side regions. The parametric edge TIF model using only the first correction (bottom left) allows us to correct the discrepancy in the edge-side removal. The removal profile based on the parametric edge TIF model using both the first and second correction (bottom right) is well matched with the experimental removal profile over the whole range of the removal profile.

This parametric edge TIF model can be used to simulate and optimize the CCOS process in the process optimization software.

2.4 Non-sequential Optimization Technique

Using well characterized TIFs, a CCOS run can be simulated and optimized. This optimization is mainly based on a de-convolution of the target removal map using the TIFs. In general, a dwell time map (i.e. ablation time as a function of position on the workpiece) is the main optimization subject for the process optimization software to achieve a given target removal map. In other words, the control intelligence uses the TIF as a building block to achieve the target removal map by spatially distributing and accumulating the TIF blocks on the workpiece.

In a conventional CCOS process, a single dwell time map of a TIF is optimized to achieve a target material removal. The convergence rate and overall efficiency of CCOS figuring are optimized using a sequence of polishing runs, where the largest scale irregularities are addressed by large tools. Smaller tools are used to correct small scale irregularities and tool marks from the larger tools. These multiple CCOS runs are optimized one by one. For instance, a large tool may be

used to address the current target removal. Then, a small tool is used to remove the remaining target removal. This method works, but may not be optimal.

The non-sequential optimization technique for the advanced CCOS process control intelligence was developed and reported in 2009 [24]. It uses multiple TIFs simultaneously in a single CCOS run optimization, while the conventional CCOS processes use TIFs in a sequential manner. The actual polishing runs are still to be sequential under the guidance of comprehensive optimization. This new technique, which enables the ensemble of various TIFs, forms an attractive solution for the mass fabrication capability of high quality optical surfaces.

3. COMPUTER CONTROLLED POLISHING MACHINES

The enhanced CCOS technologies described in Section 2 have been implemented on the computer-controlled polishing machines at the University of Arizona. RC laps using visco-elastic non-Newtonian fluids have been manufactured and used for various optical polishing projects [19-20]. The lap size varies from 100mm to 360mm in diameter. A 360mm RC lap on the 8.4m diameter GMT off-axis segment at the SOML is shown in Fig. 4.

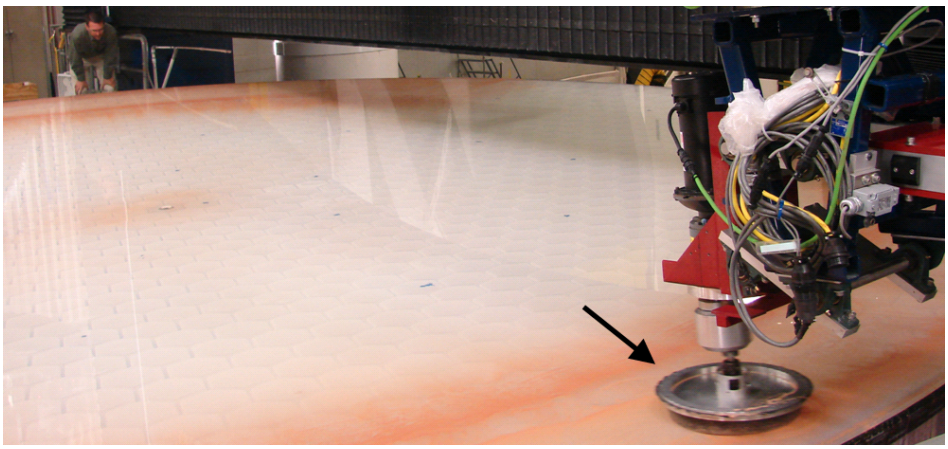

Fig. 4. The 8.4m capacity NC polishing machine equipped with 360mm diameter RC lap (black arrow) on the 8.4m diameter GMT off-axis segment at the Steward Observatory Mirror Lab [18].

Three NC polishing machines have been newly built or upgraded with the orbital tool motion generator, advanced process control intelligence software, and so forth. The orbital motion generator for the 8.4m capacity large NC polishing machine at the SOML is shown in Fig. 4 (above the RC lap). Its orbital speed and position on the workpiece are fully controlled real-time. The 4.2m capacity NC machine at the OEFF is shown with the computer control graphical user interface (GUI) in Fig. 5. The 4.2m Discovery Channel Telescope (DCT) primary mirror was successfully polished and figured on this machine [19].

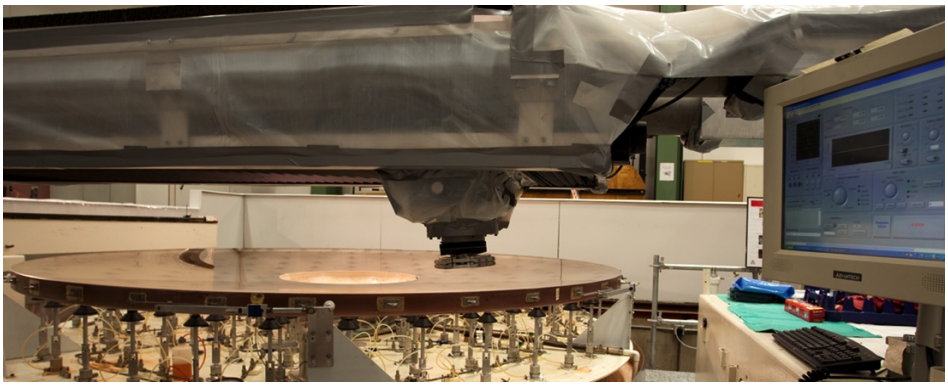

Fig. 5. The 4.2m capacity NC polishing machine at the Optical Engineering and Fabrication Facility. The GUI for automated polishing runs is shown in the computer screen. The 4.2m Discovery Channel Telescope primary mirror mounted on the supporting structures is shown [19].

The 1.8-m capacity computer controlled optical surfacing machine utilizing the swing-arm was designed and built as shown in Fig. 6. Its unique swing-arm geometry allows the polishing tool moves over the workpiece surface in an arc without additional vertical translation or tip-tilt control [9].

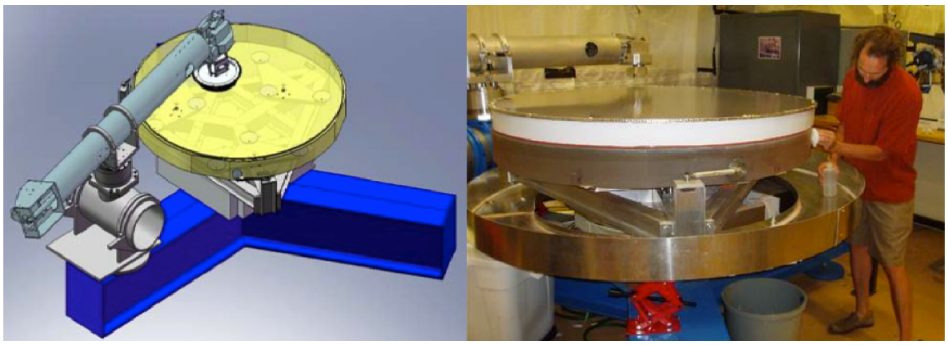

Fig. 6. The 1.8m capacity swing-arm NC polishing machine (left) developed at the Optical Engineering and Fabrication Facility. An off-axis parabola workpiece mounted on the polishing machine is shown (right) [9].

The advanced CCOS technologies in Section 2 have been embedded into the CCOS process control intelligence known as Matrix. It provides a full GUI to simulate polishing runs, including edge TIFs, to optimize the dwell time maps for a given target removal map, and to analyze and evaluate the CCOS runs by comparing the predicted and measured removal maps. A screen capture of the Matrix GUI is presented in Fig. 7.

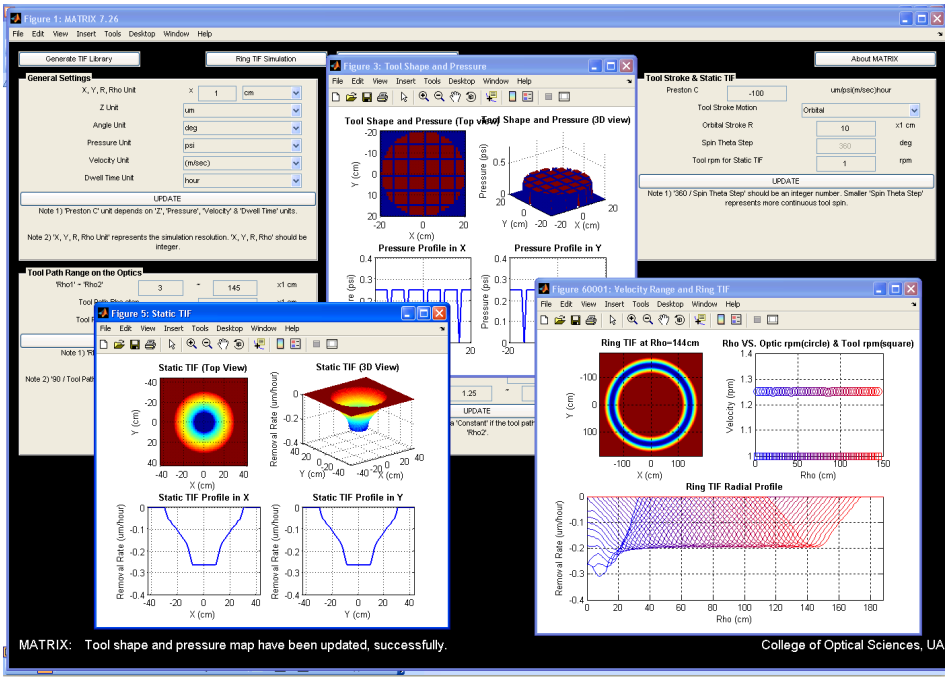

Fig. 7. Graphical user interface of Matrix, which is the CCOS process simulation and optimization software with new CCOS technologies including edge TIF model, non-sequential optimization, and so forth.

4. PERFORMANCE OF THE ADVANCED CCOS PROCESS

One of the benefits of the RC lap is the deterministic and stable TIF. Because the TIF is the basic de-convolution block for the CCOS process optimization, having a stable TIF is the key to achieve a reliable simulation result, which matches the measured result. The comparison between the theoretical TIF (based on the Preston's equation) and the measured TIF is presented in Fig. 8 [18]. This good matching is mainly due to the very uniform pressure distribution under the RC lap during the polishing tool stroke. Once the actual TIF is measured for given tool parameters (e.g. polishing pad type,

polishing compound, etc.), the Preston's coefficient κ in Eq. (1) is calibrated to fit the theoretical TIF to the measured one.

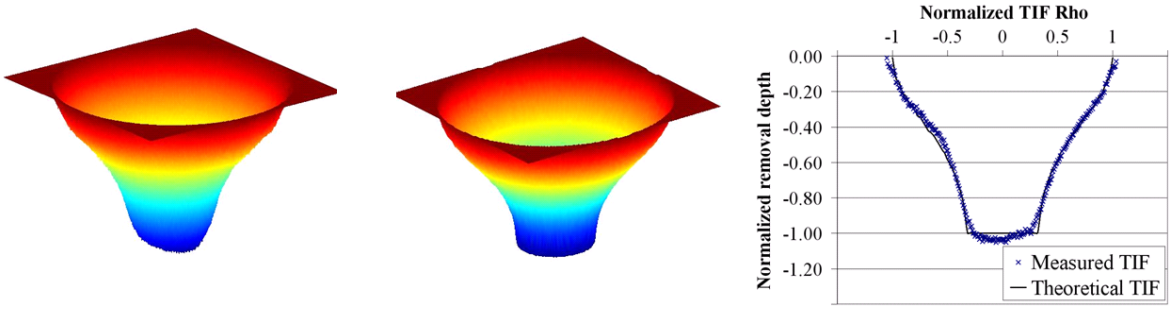

Fig. 8. TIFs using the RC lap with an orbital tool motion: measured 3D TIF (left), theoretical 3D TIF (middle), and radial profiles of them (right) [18].

Using the calibrated TIF, the process control intelligence Matrix simulates and optimizes the CCOS runs before the actual polishing. Thanks to the well calibrated TIFs and the new CCOS technologies in Matrix, the executed polishing runs have shown very deterministic results. In other words, the predicted removal map matches the measured removal map very well. The removal map refers to the difference between the surface maps before and after the polishing run.

Two polishing run results made on the 8.4m honeycomb-sandwich GMT off-axis segment are presented in Figs. 9 and 10. The off-axis segment is a highly aspheric surface, which contains 13mm peak-to-valley astigmatism [20]. The optical specifications for the segment are given in Table 1.

Table 1. Optical specifications for the 8.4m honeycomb-sandwich GMT off-axis segment [20]

Parameters	Specification
Radius of curvature R	36,000.0 $\pm$ 1.0 mm
Conic constant k	-0.998286
Off-axis distance	8710 $\pm$ 2 mm
Clocking angle	$\pm$ 50 arcseconds

Two different RC laps, 250mm and 120mm in diameter, were used during the polishing runs. The surface was measured before and after the polishing runs, and the measured removal maps were directly calculated from the surface maps. The measured removal map also includes measurement errors from the highly demanding 8.4m off-axis segment testing configuration [20]. In other words, the comparison map (i.e. measured – predicted removal map) contains not only the tool performance related errors, but also the measurement errors. For instance, the measured removal map in Fig. 10 (top left) shows non-zero values in the area with no polishing. The actual tool performance will be better than the comparison map.

The first CCOS case targeted mid- to low-frequency errors as shown in Fig. 9 (top right). The 250mm diameter RC lap was used to cover the whole 8.4m surface except the center area (the inner black circle) for 27hours. The executed dwell time map (bottom right) shows longer dwell time at higher target removal location. The predicted removal map (top right) from the Matrix program using the calibrated TIF and the dwell time map shows very good agreement with the measured removal map (top left). The comparison between the measured and the predicted removal map (bottom left) has only 97nm RMS while the measured removal map (top left) has 259nm RMS. Also, the comparison map shows very low-order mismatch (mainly trefoil), which is not similar to the target removal map (top right). This implies that measurement error (e.g. bending of the segment) is contributing to the measured removal map. Thus, the actual performance of the CCOS process will be even better.

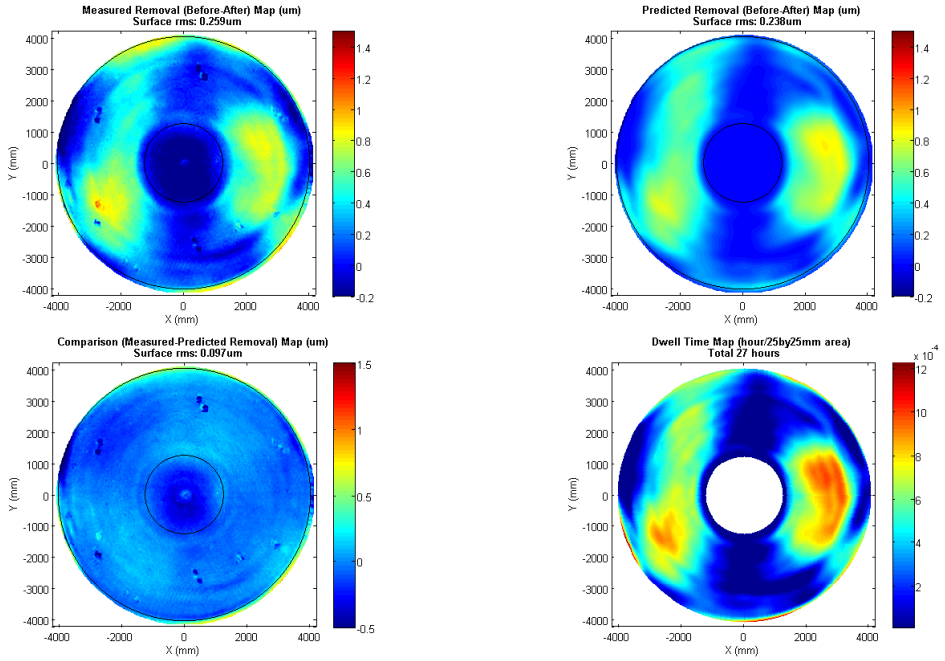

Fig. 9. Comparison (bottom left) between the measured removal map (top left) and the predicted removal map (top right) after the 27 hour CCOS run using a 250mm RC lap on the 8.4m GMT off-axis segment. Two black circles in each map represent the boundaries of the dwell time map (bottom right). The discrete points in the maps (e.g. two blue points in the 12 o'clock area of the measured removal map) are fiducial markers in the test optics, not actual surface data.

The second CCOS case was an edge figuring run as shown in Fig. 10.

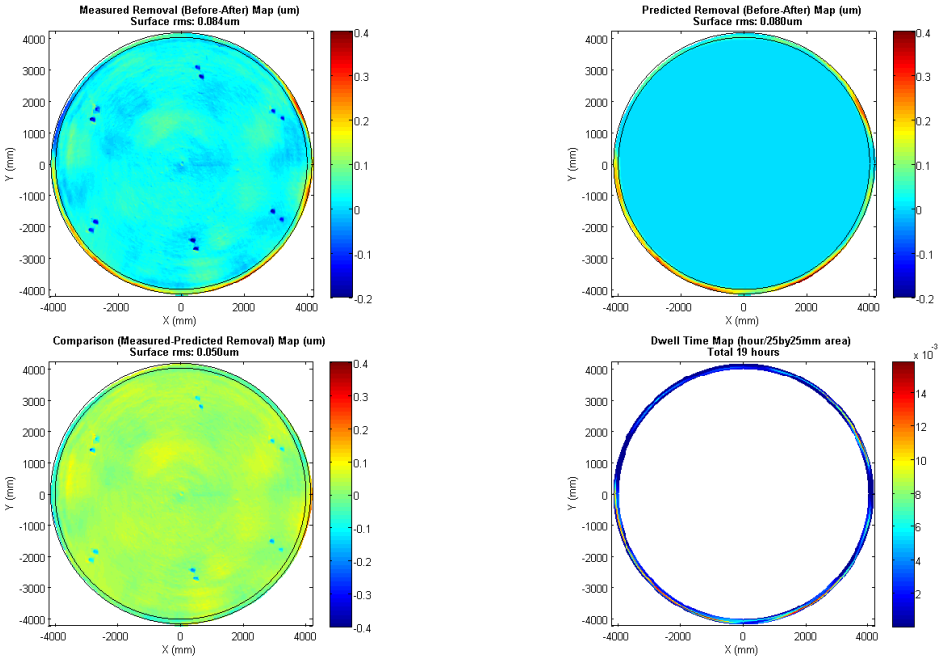

Fig. 10. Comparison (bottom left) between the measured removal map (top left) and the predicted removal map (top right) after the 19 hour CCOS run using a 120mm RC lap on the 8.4m GMT off-axis segment. Two black circles in each map represent the boundaries of the dwell time map (bottom right). The discrete points in the maps (e.g. two blue points in the 12 o'clock area of the measured removal map) are fiducial markers in the test optics, not actual surface data.

The 19 hours of polishing run time was focused exclusively on the edge area as the dwell time map (bottom right) has values only in the outer 200mm thick annular area. The 120mm diameter RC lap was used. The measured removal map (top left) shows 84nm RMS and is very similar to the predicted removal map (top right) with 80nm RMS. The comparison map shows 50nm RMS including the measurement errors.

5. CONCLUDING REMARKS

The University of Arizona has successfully demonstrated advanced capability for manufacturing non-symmetrical aspheric optical surfaces with the 8.4m GMT off-axis segment polishing run results. These advanced CCOS technologies, including the RC lap, parametric models for smoothing and edge TIFs, and the non-sequential optimization technique, provide powerful means to optimize and design a CCOS process. For instance, a highly aspheric optical surface can be efficiently manufactured using a few different sizes of RC laps without being limited by tool-workpiece misfit. The good match between measured and predicted removal maps enables more reliable CCOS process optimization. These enhanced features give us the highest optical surface qualities with improved convergence rate. This CCOS process will be used for the next generation of optical systems including GMT, the Large Synoptic Survey Telescope (LSST), and the Advanced Technology Solar Telescope (ATST) at the University of Arizona.

6. ACKNOWLEDGEMENT

This material is based in part upon work supported by AURA through the National Science Foundation under Scientific Program Order No. 10 as issued for support of the Giant Segmented Mirror Telescope for the United States Astronomical Community, in accordance with Proposal No. AST-0443999 submitted by AURA.

REFERENCES

[1] R. A. Jones, “Computer control for grinding and polishing,” Photonics Spectra, 34-39 (1963).
[2] R. Aspden, R. McDonough, and F. R. Nitchie, Jr, “Computer assisted optical surfacing,” Applied Optics. 11, 2739-2747 (1972).
[3] R. E. Wagner and R. R. Shannon, “Fabrication of aspherics using a mathematical model for material removal,” Applied Optics. 13, 1683-1689 (1974).
[4] R. A. Jones, “Computer-controlled polishing of telescope mirror segments,” Optical Engineering. 22, 236-240 (1983).
[5] R. A. Jones, “Computer-controlled optical surfacing with orbital tool motion,” Optical Engineering. 25, 785-790 (1986).
[6] J. R. Johnson and E. Waluschka, “Optical fabrication-process modeling-analysis tool box,” in Manufacturing and metrology tooling for the Solar-A Soft X-Ray Telescope, W.R. Sigman, L.V. Burns, C.G. Hull-Allen, A.F. Slomba, and R.G. Kusha, eds., Proc. SPIE 1333, 106-117 (1990).
[7] D. D. Walker, D. Brooks, A. King, R. Freeman, R. Morton, G. McCavana, and S.W. Kim, “The ‘Precessions’ tooling for polishing and figuring flat, spherical and aspheric surfaces”, Opt. Express, 11, 958-964 (2003).
[8] H. M. Pollicove, E. M. Fess, and J. M. Schoen, “Deterministic manufacturing processes for precision optical surfaces,” in Window and Dome Technologies VIII, R. W. Tustison, eds., Proc. SPIE 5078, 90-96 (2003).
[9] J. H. Burge, S. Benjamin, D. Caywood, C. Noble, M. Novak, C. Oh, R. Parks, B. Smith, P. Su, M. Valente, and C. Zhao, “Fabrication and testing of 1.4-m convex off-axis aspheric optical surfaces,” in Optical Manufacturing and Testing VIII, J. H. Burge; O. W. Fähnle and R. Williamson, eds., Proc. SPIE 7426, 74260L1-12 (2009).
[10] J. Nelson and G. H. Sanders, “The status of the Thirty Meter Telescope project,” in Ground-based and Airborne Telescopes II, L. M. Stepp and R. Gilmozzi, eds., Proc. SPIE 7012, 70121A1-18 (2008).
[11] A. Ardeberg, T. Andersen, J. Beckers, M. Browne, A. Enmark, P. Knutsson and M. Owner-Petersen, “From Euro50 towards a European ELT,” in Ground-based and Airborne Telescopes, L. M. Stepp, eds., Proc. SPIE 6267, 626725 1-10 (2006).
[12] A. Heller, “Safe and sustainable energy with LIFE,” https://str.llnl.gov/AprMay09/pdfs/05.09.02.pdf (2009).
[13] M. Johns, “The Giant Magellan Telescope (GMT),” in Extremely Large Telescopes: Which Wavelengths?, T. E. Andersen, eds., Proc. SPIE 6986, 698603 1-12 (2008).
[14] A. Swat, “Specifications for the feasibility study of the polishing of the E-ELT primary mirror segments, constant gap case,” in E-ESO-SPE-300-0048 Issue 1 (2007).

[15] R. E. Parks, “Specifications: Figure and Finish are not enough,” in An optical Believe It or Not: Key Lessons Learned, M. A. Kahan, eds., Proc. SPIE 7071, 70710B1-9 (2008).
[16] J. M. Hill, “Optical Design, Error Budget and Specifications for the Columbus Project Telescope,” in Advanced Technology Optical Telescopes IV, L. D. Barr, eds., Proc. SPIE 1236, 86-107 (1990).
[17] M. T. Tuell, J. H. Burge, B. Anderson, “Aspheric optics: smoothing the ripples with semiflexible tools,” Opt. Eng. 41 1473-1474 (2002).
[18] D. W. Kim and J. H. Burge, “Rigid conformal polishing tool using non-linear visco-elastic effect,” Opt. Express. 18, 2242-2257 (2010)
[19] M. J. Valente, D. W. Kim, M. J. Novak, C. J. Oh, J. H. Burge, “Fabrication of 4-meter class astronomical optics,” Proc. SPIE 7739, (2010).
[20] H. M. Martin, R. G. Allen, J. H. Burge, D. W. Kim, J. S. Kingsley, M. T. Tuell, S. C. West, C. Zhao and T. Zobrist, “Fabrication and testing of the first 8.4 m off-axis segment for the Giant Magellan Telescope,” Proc. SPIE 7739, (2010)
[21] D. W. Kim, W. H. Park, H. K. An, and J. H. Burge, “Parametric smoothing model for visco-elastic polishing tools,” Opt. Express 18, 22515-22526 (2010)
[22] D. W. Kim, W. H. Park, S. W. Kim, and J. H. Burge, “Parametric modeling of edge effects for polishing tool influence functions,” Opt. Express. 17, 5656-5665 (2009).
[23] D. W. Kim, W. H. Park, S. W. Kim, and J. H. Burge, “Edge tool influence function library using the parametric edge model for computer controlled optical surfacing,” in Optical Manufacturing and Testing VIII, J. H. Burge; O. W. Fähnle and R. Williamson, Proc. SPIE 7426, 74260G1-12 (2009).
[24] D. W. Kim, S. W. Kim, and J. H. Burge, “Non-sequential optimization technique for a computer controlled optical surfacing process using multiple tool influence functions,” Opt. Express. 17, 21850-21866 (2009).
[25] D. W. Kim, “Next Generation Computer Controlled Optical Surfacing,” PhD Dissertation (2009).